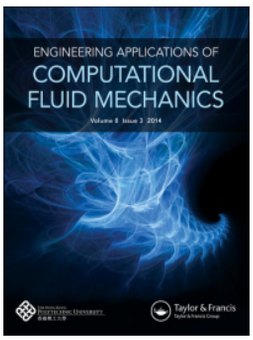

Taylor & Francis
Taylor & Francis Group

Engineering Applications of Computational Fluid Mechanics

ISSN: (Print) (Online) Journal homepage: https://www.tandfonline.com/loi/tcfm20

Role of gradients and vortexes on suitable location of discrete heat sources on a sinusoidal-wall microchannel

Liang Cheng, Yufang Zhu, Shahab S. Band, Dariush Bahrami, Rasool Kalbasi, Arash Karimipour, Mehdi Jahangiri, Kwok-Wing Chau & Amir Mosavi

To cite this article: Liang Cheng, Yufang Zhu, Shahab S. Band, Dariush Bahrami, Rasool Kalbasi, Arash Karimipour, Mehdi Jahangiri, Kwok-Wing Chau & Amir Mosavi (2021) Role of gradients and vortexes on suitable location of discrete heat sources on a sinusoidal-wall microchannel, Engineering Applications of Computational Fluid Mechanics, 15:1, 1176-1190, DOI: 10.1080/19942060.2021.1953608

To link to this article: https://doi.org/10.1080/19942060.2021.1953608

Published online: 06 Aug 2021.

ENGINEERING APPLICATIONS OF COMPUTATIONAL FLUID MECHANICS
2021, VOL. 15, NO. 1, 1176–1190
https://doi.org/10.1080/19942060.2021.1953608

Taylor & Francis
Taylor & Francis Group

Role of gradients and vortexes on suitable location of discrete heat sources on a sinusoidal-wall microchannel

Liang Cheng[a,b], Yufang Zhu[c], Shahab S. Band[d], Dariush Bahrami[e], Rasool Kalbasi[f], Arash Karimipour[f], Mehdi Jahangiri[g], Kwok-Wing Chau[h] and Amir Mosavi[i,j,k]

[a]College of Chemical Engineering, Guangdong University of Petrochemical Technology, Maoming, Guangdong, People's Republic of China; [b]Key Laboratory of Inferior Crude Oil Processing of Guangdong Provincial Higher Education Institutes, Maoming, Guangdong, People's Republic of China; [c]School of Information Science and Technology, South China Business College, Guangdong University of Foreign Studies, Guangzhou, Guangdong, People's Republic of China; [d]Future Technology Research Center, College of Future, National Yunlin University of Science and Technology, Douliou, Yunlin, Taiwan; [e]Department of Mechanical Engineering, Shahrekord University, Shahrekord, Iran; [f]Department of Mechanical Engineering, Najafabad Branch, Islamic Azad University, Najafabad, Iran; [g]Department of Mechanical Engineering, Shahrekord Branch, Islamic Azad University, Shahrekord, Iran; [h]Department of Civil and Environmental Engineering, Hong Kong Polytechnic University, Hong Kong, People's Republic of China; [i]Faculty of Civil Engineering, Technische Universität Dresden, Dresden, Germany; [j]John von Neumann Faculty of Informatics, Obuda University, Budapest, Hungary; [k]Department of informatics, J. Selye University, Komarom, Slovakia

ABSTRACT

The idea of using the compact device with higher heat transfer potential has encouraged researchers to use microchannels. Creating sinusoidal walls is a technique leading to better effectiveness and smaller size. In this study, the effects of discrete heat sources location on heat transfer and pressure drop are investigated, using graphene nanoplatelets/water inside a sinusoidal microchannel. For this, discrete heat sources are installed in a smooth microchannel (layout A) and compared with two sinusoidal-wall microchannels. In layouts B and C, the heating sources are installed above the convergent/diverging sections, respectively. Since the velocity and temperature gradients are higher in the converging region, the heat exchange and pressure drop for layout B are greater than other ones. In other words, installing heating sources in these regions with high-temperature gradient has a more obvious positive efficacy on heat exchange. For the best layout (B), although the heat exchange compared to the base layout (A) is 37.5% higher, the pressure drop and entropy generation are higher by 79% and 35.2%, respectively. By introducing a new figure of merit (FOM), it is found that layout B is in the desirable zone.

ARTICLE HISTORY
Received 8 September 2020
Accepted 25 June 2021

KEYWORDS
Microchannel; discrete heat sources; sinusoidal-wall; entropy generation; vortex

1. Introduction

Focusing on heat exchange has been one of the most significant topics in various researches as well as industries. There are several ways to improve heat transfer (Bakthavatchalam et al., 2020). Material science and nanotechnology result in remarkable advancement in heat transfer (Abedi et al., 2016; Kuskov et al., 2021). Higher heat exchange potential along with the compact design are unique properties of microchannels (Akbari et al., 2016; Gravndyan et al., 2017). A very effective solution in modern science is to utilize microchannels. Microchannels have a wide range of applicants in microfluidic devices (D. Bahrami et al., 2020). Many researchers investigated the microchannel effectiveness (Heydari et al., 2017; Shamsi et al., 2017). Ravi et al. (2017) investigated heat exchange within a channel using four rib configurations and showed that the highest heat exchange, as well as the highest pressure drop (ΔP), were attributed to the V-shape rib. Min et al. (2020) optimized the rib geometric profile within a rectangular channel to achieve the maximum heat exchange and simultaneously minimum ΔP. They proved that the adopted profile had higher heat exchange and less ΔP than the rectangular one. Al Kumait et al. (2019) investigated the effects of rib angle (installed inside the tube) on nanofluid heat exchange numerically and experimentally. They found that increasing the nanoparticles volume fraction (φ_{np}) and Reynolds number intensified heat exchange. They also reported that the performance of the spiral tube was 2% higher compared with that of the simple tube. Other researchers used porous media (Xu et al., 2019) to improve heat exchange. Shen et al. (2017) studied the effects of metal foam porosity on heat exchange and ΔP inside the microchannel. They used different metal foam arrangements and revealed that installing metal foam had a greater effect on ΔP than heat exchange.

CONTACT Shahab S. Band shamshirbands@yuntech.edu.tw; Amir Mosavi amir.mosavi@mailbox.tudresden.de

A discrete heating source has been considered by researchers in many studies. Ren et al. (2019) studied the natural heat exchange from the solar chimney equipped with discrete heating sources. The results showed that the adopted solar chimney had a better performance than the conventional one. Babajani et al. (2017) numerically investigated mixed convection heat exchange of nanofluid flow inside a two-dimensional channel with four discrete heat sources. They reported that increasing φ_{np} intensifies heat exchange and the intensity of temperature gradient near the heating sources. Sankar and Do (2010) studied convection heat exchange inside a vertical cylinder with two discrete heat sources on the wall. Using finite element, it was reported that heat exchange was directly related to the radial ratio and inversely related to the aspect ratio. Shiriny et al. (2019) investigated the effect of heating source installation on heat exchange in a microchannel equipped with triangular ribs. By installing heating sources in the flow direction, it was found that if the slip coefficient increased, the heat exchange would improve. By installing heating sources behind triangular ribs, heat exchange was reduced with an increasing slip coefficient. Toghraie et al. (2019) investigated the effectiveness of a double pipe heat exchanger in two scenarios. In the first scenario, the heat flux was applied continuously and in the second one, the heat exchange was applied discontinuously. The results showed that the heat exchanger effectiveness in the second scenario was higher. A. Bahrami et al. (2020) investigated heat exchange inside a microchannel equipped with a discrete heating source. Considering laminar flow, they used several nanofluids and revealed that if the heat sources were installed opposite the top and bottom of the microchannel, the temperature of the nanofluid in the middle of the microchannel is maximized. They reported that at Re = 30, the rate of heat exchange in the opposite array was 6% more than face to face array.

Dinarvand et al. (2021) considered the effect of magnetic field on the thermal and hydrodynamic boundary layer. They claimed that increasing magnetic strength resulted in a lower thermal and hydrodynamic boundary thickness and subsequently improvement of heat exchange. Using heat exchange improvement techniques also affected entropy generation $\dot{s}_{gen}$. In general, $\dot{s}_{gen}$ was divided into a viscous term as well as a thermal one. The former was generated due to frictional force and the latter was attributed to heat exchange (Chen et al., 2019; Huminic & Huminic, 2020). Esfahani et al. (2017) investigated $\dot{s}_{gen}$ in a sinusoidal plate heat exchanger. They reported that $\dot{s}_{gen}$ was zero at the center and approaches of the heat exchanger and that its maximum value was at the lateral wall. Karimipour et al. (2020) investigated the effect of injection on entropy generation in a microchannel. Their result alleged that injection brought out both thermal and viscous entropy generations. Leong et al. (2012) studied heat exchange and $\dot{s}_{gen}$ inside a helical heat exchanger. They found that the lowest $\dot{s}_{gen}$occurred at an angle of 50° and the highest heat exchange occurred at 25°. Nguyen et al. (2020) studied a double pipe sinusoidal-wavy wall heat exchanger from the first law as well as the second law of thermodynamics. They applied magnetic field in the presence of FMWCNT/water. Under the best conditions, using sinusoidal-wavy wall could increase heat exchange by 19% while $\dot{s}_{gen}$ was intensified by 8%. Dormohammadi et al. (2018) studied $\dot{s}_{gen}$ inside a wavy-wall channel with nanofluid. They reported that the lowest thermal entropy as well as viscous entropy generation occurred at a certain amplitude, and increasing φ_{np} diminished $\dot{s}_{gen}$. Akbarzadeh et al. (2019) studied nanofluid flow inside a wavy-wall heat exchanger containing porous media from the first and second laws. They revealed that in the divergent section of the sinusoidal duct, the temperature of the nanofluid was higher than that in the convergent section. On the other hand, thermal entropy generation in the divergent section was greater than that in the convergent section (Table 1).

Literature review revealed that several studies were performed on microchannel. However, no study has been conducted on the effects of installation layout of discrete heating sources in a sinusoidal-wall microchannel. Therefore, in this study, three discrete heating sources are installed in a sinusoidal-wall microchannel equipped with nanofluid. By changing the heating source installation location from the converging section to the diverging one, heat exchange is examined in order to obtain a suitable layout. Eventually, from the second law of thermodynamics, the effects of installation location on $\dot{s}_{gen}$are evaluated.

2. Problem description

The problem geometry is illustrated in Figure 1. The microchannel length and width are 40,000 and 1000 μm, respectively. The parameters of l_1, l_2, l_3 and l_4 are considered to be 10,000, 400, 400 and 10,000 μm. As shown in Figure 1, the bottom and upper walls are obtained from $S(X) = \pm 0.5 \sin\left(\frac{\pi X}{4}\right)$ where X varies in the range 10–30.

$$\left\{L - \left(\frac{l_1}{h} + \frac{l_2}{h} + \frac{l_3}{h} + \frac{l_4}{h}\right)\right\}$$

Laminar flow of nanofluid enters the microchannel with an initial temperature of 293 K and leaves the microchannel after heat transferring with discrete heating sources at $T_h = 313$K. Table 2 reports thermophysical properties of nanofluids.

Table 1. Studies focusing on heat exchange and $\dot{s}_{gen}$.

Authors	Problem	Effect of	funding
Bahiraei et al. (2019)	Tube	• Twisted tape inserts • Loading nanofluid	• Decreasing the twisted ratio from 3.5 to 2.5 led to 10% decrement in thermal entropy generation • Adding nanoparticle led to 14% decrease in thermal entropy generation
Li et al. (2020)	Sinusoidal hairpin heat exchanger	Using hybrid nanofluid	By growing φ, at Re = 1000 and Re = 1500 entropy generation reduced, while at Re = 100 and Re = 500, it was increased
Vatanparast et al. (2020)	Rectangular channel	Staggered semi-porous fins	• At higher Darcy number, less total entropy generation • 44% increment in $\dot{s}_{gen}$ due to increasing Re from 50 to 1000
Kurnia et al. (2016)	Helical and straight tube	Various cross section	• Square tube has more $\dot{s}_{gen}$ as compared to ellipse and circular cross-section
Rashidi et al. (2017)	Eccentricity tube	Screw tape insert	• 42% growth in viscous entropy generation for eccentricity in the range of 0–3.5 • 237% intensification for eccentricity in the range of 0–3.5

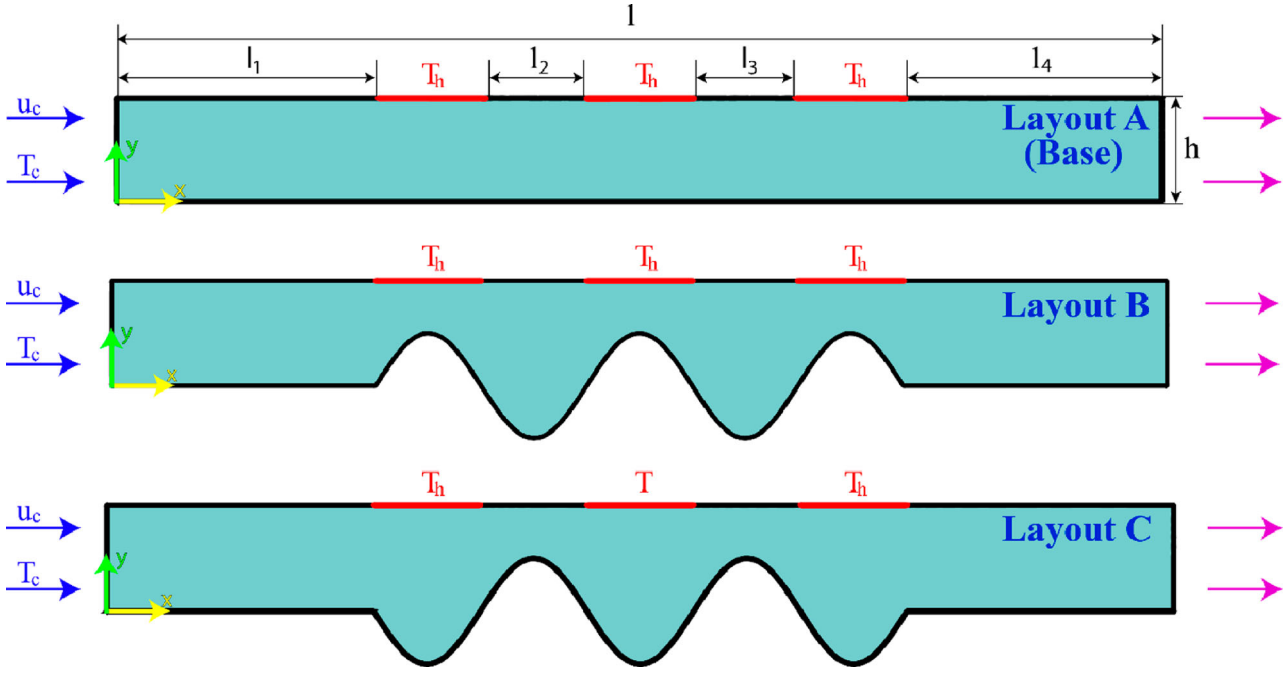

Figure 1. Different layouts of discrete heating sources.

3. Governing equations

Numerical method is applied to solve continuity (Equation (1)), momentum (Equations (2) and (3)) and energy (Equation (4)) equations, in which the nanofluid is considered steady, incompressible, and laminar at single phase (Mazaheri et al., 2019):

$$\frac{\partial u}{\partial x} + \frac{\partial v}{\partial y} = 0 \tag{1}$$

Table 2. Properties of graphene nanoplatelet/water nanofluids (Mazaheri et al., 2019).

ϕ(%)	Viscosity (Pa · s)	Specific heat (J/kg · K)	Thermal conductivity (W/m · K)	Density (kg/m^3)
0	$3.08212404044923 \times 10^{13} \times T^{-6.6681}$	$0.12T + 4065.8$	$0.0020338T - 0.0057$	$1085.05 - 0.29689T$
0.06	$7.04657066469 \times 10^{7} \times T^{-4.366}$	$4248.1 - 0.77771T$	$0.0029T - 0.2336$	$1085.1 - 0.2943T$
0.1	$3.5197010825669 \times 10^{8} \times T^{-4.63845}$	$1.02T + 3492.5$	$0.0032T - 0.2646$	$1086.5 - 0.2979T$

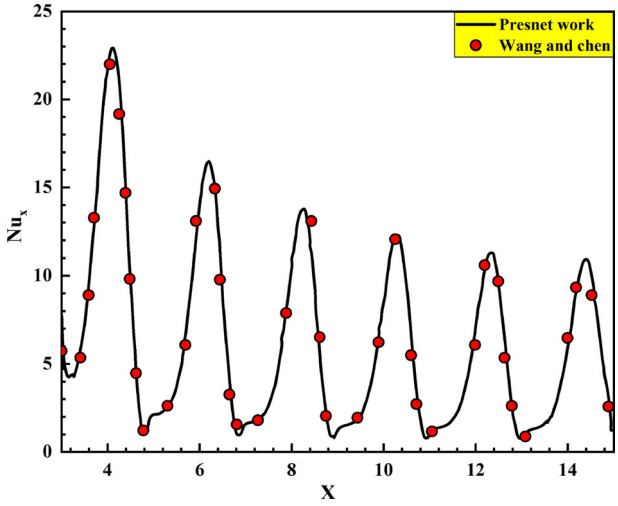

Figure 2. Validation by comparing the results of Wang and Chen (2002) with the present numerical method.

$$u\frac{\partial u}{\partial x}+v\frac{\partial u}{\partial y}=-\frac{1}{\rho_{\mathrm{nf}}}\frac{\partial p}{\partial x}+\frac{\mu_{\mathrm{nf}}}{\rho_{\mathrm{nf}}}\left(\frac{\partial^2 u}{\partial x^2}+\frac{\partial^2 u}{\partial y^2}\right) \quad (2)$$

$$v\frac{\partial v}{\partial x}+v\frac{\partial v}{\partial y}=-\frac{1}{\rho_{\mathrm{nf}}}\frac{\partial p}{\partial y}+\frac{\mu_{\mathrm{nf}}}{\rho_{\mathrm{nf}}}\left(\frac{\partial^2 v}{\partial x^2}+\frac{\partial^2 v}{\partial y^2}\right) \quad (3)$$

$$u\frac{\partial T}{\partial x}+v\frac{\partial T}{\partial y}=\alpha_{\mathrm{nf}}\left(\frac{\partial^2 T}{\partial x^2}+\frac{\partial^2 T}{\partial y^2}\right) \quad (4)$$

In the continuity and momentum equations, x and y denote horizontal and vertical distances, respectively, and u and v are horizontal and vertical velocity $\left(\frac{\mathrm{m}}{\mathrm{s}}\right)$, respectively. In the momentum equations, μ_{nf} is the viscosity of nanofluid (Pa·s) and p is pressure (Pa). For the energy equation, T is the temperature (K), $\alpha_{\mathrm{nf}}=\frac{k_{\mathrm{nf}}}{\rho_{\mathrm{nf}}C_{\mathrm{nf}}}$ defines the thermal diffusivity $\left(\frac{\mathrm{m}^2}{\mathrm{s}}\right)$, in which k_{nf}, ρ_{nf}, and C_{nf} are the thermal conductivity $\left(\frac{\mathrm{W}}{\mathrm{m}\cdot\mathrm{K}}\right)$, density $\left(\frac{\mathrm{kg}}{\mathrm{m}^3}\right)$, and heat capacity of nanofluid $\left(\frac{\mathrm{J}}{\mathrm{kg}\cdot\mathrm{K}}\right)$, respectively.

To write continuity, momentum and energy equations in dimensionless form, the following parameters are utilized:

$$X=\frac{x}{h},Y=\frac{y}{h},U=\frac{u}{u_c},V=\frac{v}{u_c},H=\frac{h}{h},L=\frac{l}{h} \quad (5)$$

$$\theta=\frac{T-T_c}{T_h-T_c},P=\frac{\bar{p}}{\rho_{\mathrm{nf}}{u_c}^2},\mathrm{Re}=\frac{u_c h}{\vartheta_{\mathrm{nf}}},\mathrm{Pr}=\frac{\vartheta_{\mathrm{nf}}}{\alpha_{\mathrm{nf}}}$$

Non-dimensionless continuity, momentum in x and y directions and energy equations are written in Equations (6)–(10), respectively:

$$\frac{\partial U}{\partial X}+\frac{\partial V}{\partial Y}=0 \quad (6)$$

$$U\frac{\partial U}{\partial X}+V\frac{\partial U}{\partial Y}=-\frac{\partial P}{\partial X}+\frac{\vartheta_{\mathrm{nf}}}{\vartheta_f\mathrm{Re}}\left(\frac{\partial^2 U}{\partial X^2}+\frac{\partial^2 U}{\partial Y^2}\right) \quad (7)$$

$$U\frac{\partial V}{\partial X}+V\frac{\partial V}{\partial Y}=-\frac{\partial P}{\partial Y}+\frac{\vartheta_{\mathrm{nf}}}{\vartheta_f\mathrm{Re}}\left(\frac{\partial^2 V}{\partial X^2}+\frac{\partial^2 V}{\partial Y^2}\right) \quad (8)$$

$$U\frac{\partial \theta}{\partial X}+V\frac{\partial \theta}{\partial Y}=\frac{\alpha_{\mathrm{nf}}}{\alpha_f\mathrm{Re}\cdot\mathrm{Pr}}\left(\frac{\partial^2 \theta}{\partial X^2}+\frac{\partial^2 \theta}{\partial Y^2}\right) \quad (9)$$

It should be mentioned that all equations are obtained according to the following boundary conditions:

out flow	$\frac{\partial\theta}{\partial X}=0,\frac{\partial U}{\partial X}=0,V=0,P=0$ at $(X=\mathrm{L},0\le Y\le 1)$
down wall	$\theta=0,U=0,V=0$ at $Y=0,0\le X\le L$
up wall	$\left\{\begin{array}{c}\theta=1,U=0,V=0\text{ at }Y=1,\left(L-\left(\frac{l_1}{h}+\frac{l_2}{h}+\frac{l_3}{h}+\frac{l_4}{h}\right)\right)\\ \theta=0,U=0,V=0\text{ at }Y=1,\left(\frac{l_1}{h}+\frac{l_2}{h}+\frac{l_3}{h}+\frac{l_4}{h}\right)\end{array}\right\}$
inflow	$\theta=0,\ U=1,V=0\ at x=0,\ 0<\mathrm{Y}<1$

Since some parts of the up wall are insulated and other parts are at constant temperature, it is divided into two parts.

Nusselt number is presented to show heat exchange with the following equations:

$$\mathrm{Nu}_x=-\frac{k_{\mathrm{nf}}}{k_f}\left(\frac{\partial\theta}{\partial Y}\right)_{Y=0,1} \quad (10)$$

$$\overline{\mathrm{Nu}}=\frac{1}{L}\int_0^L \mathrm{Nu}_x dX \quad (11)$$

To simultaneously investigate heat exchange and ΔP, a performance evaluation criterion (PEC) parameter is introduced as follows (Yang et al., 2020):

$$\mathrm{PEC}=\frac{\left(\frac{\mathrm{Nu}}{\mathrm{Nu}_{\mathrm{base}}}\right)}{\left(\frac{\Delta P}{\Delta P_{\mathrm{base}}}\right)^{\frac{1}{3}}} \quad (12)$$

Pumping power, depending on ΔP, is determined with the following equations (Ebrahimi et al., 2015):

$$\text{Pumping power}=\text{volumetric flow}\times\Delta P(\mathrm{W}) \quad (13)$$

$\dot{s}_{\mathrm{gen}}$includes thermal and viscous terms, which are computed from Equations (14) and (15) (Akar et al.,

Figure 3. Distribution of computational meshes.

Table 3. Grid study.

Model	Grid number	$\mathrm{Nu}_{\mathrm{ave}}$	Error%
A	1220	5.0768	–
B	3840	5.59	10.1
C	22,000	5.79	3.577
D	44,000	5.76	0.518
E	65,000	5.77	0.173

2018):

$$\dddot{S}_{\text{th}} = \frac{k_{\text{nf}}}{T^2}\left[\left[\left(\frac{\partial T}{\partial x}\right)^2 + \left(\frac{\partial T}{\partial y}\right)^2\right]\right] \quad \left(\frac{\text{W}}{\text{m}^3 \cdot \text{K}}\right) \tag{14}$$

$$\dddot{S}_f = \frac{\mu_{\text{nf}}}{T}\left[2\left[\left(\frac{\partial u}{\partial x}\right)^2 + \left(\frac{\partial v}{\partial y}\right)^2\right] + \left(\frac{\partial u}{\partial y} + \frac{\partial v}{\partial x}\right)^2\right] \left(\frac{\text{W}}{\text{m}^3 \cdot \text{K}}\right) \tag{15}$$

Integrating from Equations (14) and (15) can specify global entropy generation per unit depth in the entire domain of fluid:

$$\dot{S} = \int \dddot{S} dA \quad \left(\frac{\text{W}}{\text{m} \cdot \text{K}}\right) \tag{16}$$

$\dot{s}_{\text{gen}}$can be rewritten in dimensionless form as follows:

$$\dddot{N} = \frac{\dddot{S} \cdot h^2}{k_f} \tag{17}$$

$$\dot{N} = \frac{1}{A}\int \dddot{N} \cdot dA \tag{18}$$

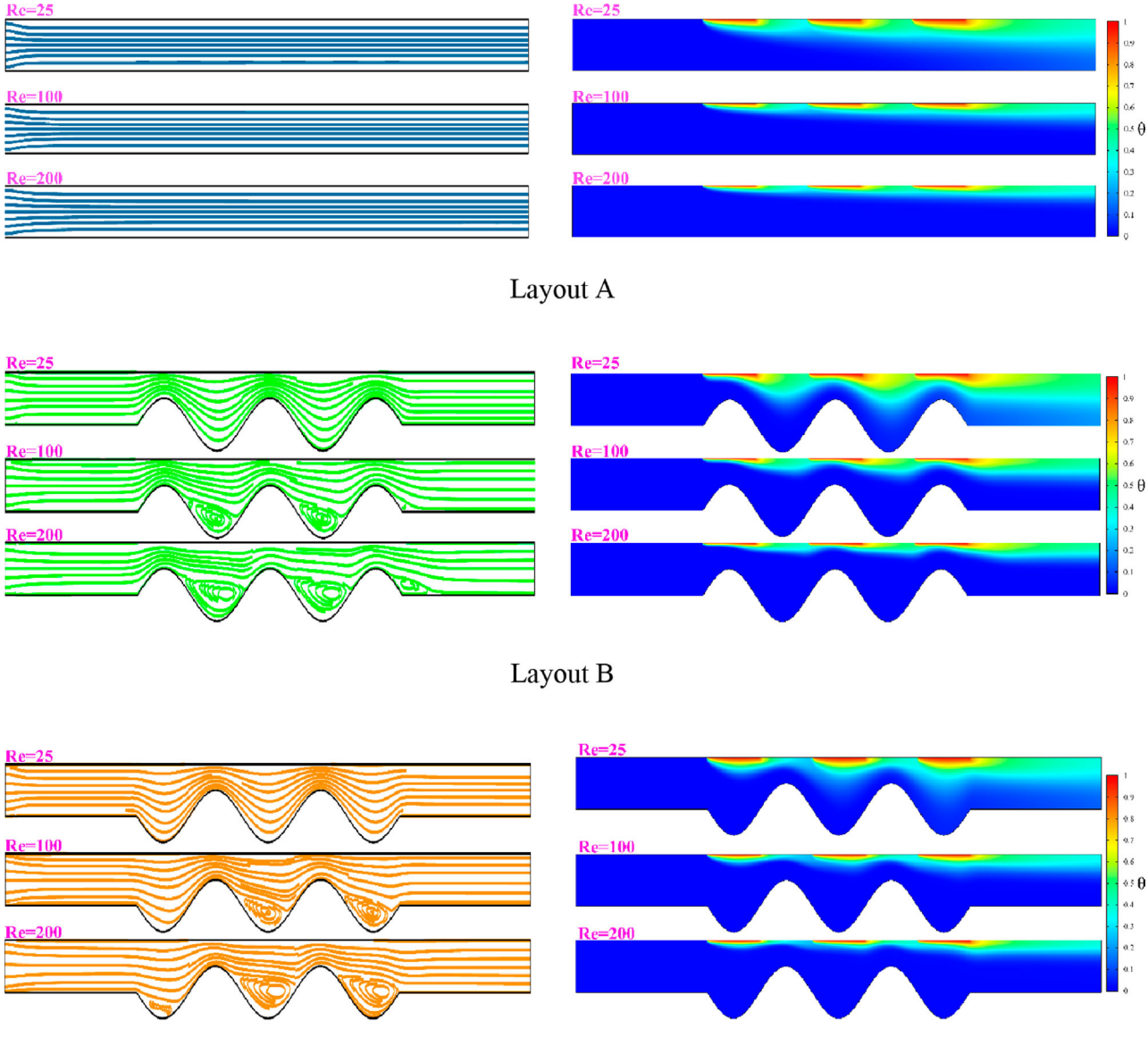

Figure 4. Streamlines and isotherm lines in various layouts.

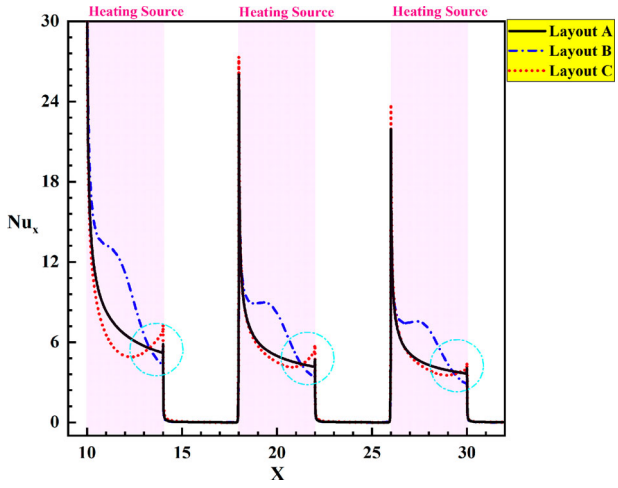

Figure 5. Variation in Nu_m at Re = 100.

4. Numerical approaches and validation

In this study, finite volume method with second-order discretization is implemented for continuity, momentum and energy equations. Moreover, the SIMPLE algorithm is used to couple pressure and velocity. For validation, the results obtained for a sinusoidal-wall microchannel are used (Wang & Chen, 2002). The variations of local Nusselt numbers are compared for validation and it is found that the present numerical approach can well simulate microchannel heat exchange (Figure 2).

To reduce the running time and boosting accuracy, structured meshes are used within the microchannel. As illustrated in Figure 3, finer meshes are applied to the heating source regions where the temperature gradient is higher. According to Table 3, five networks (A, B, C, D, and E) are used to examine the independence of the solution. As the number of computational cells increases, the sensitivity of Nu_{ave} to the number of meshes drops. By increasing the number of cells from 44,000 to 65,000, Nu_{ave} experiences a decrease of 0.173%, which can be ignored, and therefore network D is used for performing the rest of simulations.

5. Results and discussion

As mentioned, the main purpose of this study is to examine the effects of using different heat source layouts (as shown in Figure 1) on heat exchange so that the highest heat exchange rate occurs between the nanofluid and the sinusoidal-wall microchannel.

5.1. Streamlines distribution

Figure 4 shows streamlines as well as isotherm lines in layouts A, B, and C. As can be seen, in lower Reynolds number, vortex is not formed and the nanofluid is moving directly. As the Reynolds number increases, vortex forms just behind the peaks in layout B and C, while no vortex is formed in layout A.

5.2. Local Nusselt number

Figure 5 presents local Nusselt number variations. As it is shown, in adiabatic regions, the local Nusselt is zero. Upon entering regions where heating sources are installed, the local Nusselt has a sudden increase and then decreases. It can be seen the local Nusselt for layout B is more than that for others. It is because the temperature gradient for this layout is higher (as shown in Figure 4).

5.3. Average Nusselt number

Figure 6 shows the variation of Nu_m at 0, 0.06 and 0.1 vol.%. As it is depicted, increasingRe results in rising of the average Nusselt number for all layouts. Note that increasing Re increases the thickness of the thermal boundary layer as well as temperature gradient, which consequently enhances heat exchange. At 0, 0.06, and 0.1 vol.%, the performance of layout B is better than that of others. It is because, in layout B, the streamlines intensity in the region close to heating source (as shown in Figure 4) is higher. More streamlines intensity implies a higher temperature gradient and consequently better heat exchange.

Figure 6 shows that layout B has better heat exchange than base layout (A). In other words, by installing heating source in the converging section of a sinusoidal-wall, heat exchange can be improved by 37.5%. However, by installing heating sources in the diverging section, it cannot be expected that heat exchange will always be improved. With increasing Re up to 150, layout A performs better than layout C, while with further increase of Re, the behavior is quite the opposite. Undoubtedly, this can be attributed to the presence of vortex. As mentioned in Figure 4, at low Re, vortex does not form. In this case, the intensity of streamlines in layout A is higher than that in layout C and consequently heat exchange in the former is higher than that in the latter. With the increase of Re, vortexes form and their strength intensify and direct streamlines upwards (close to heating sources). In other words, they increase the streamline intensity, and therefore it can be claimed that the temperature gradient in layout C becomes greater than that in layout A, which consequently intensifies heat exchange. Under the best conditions, by installing heating source in the diverging section of a sinusoidal-wall, heat exchange can be improved by 3.7%.

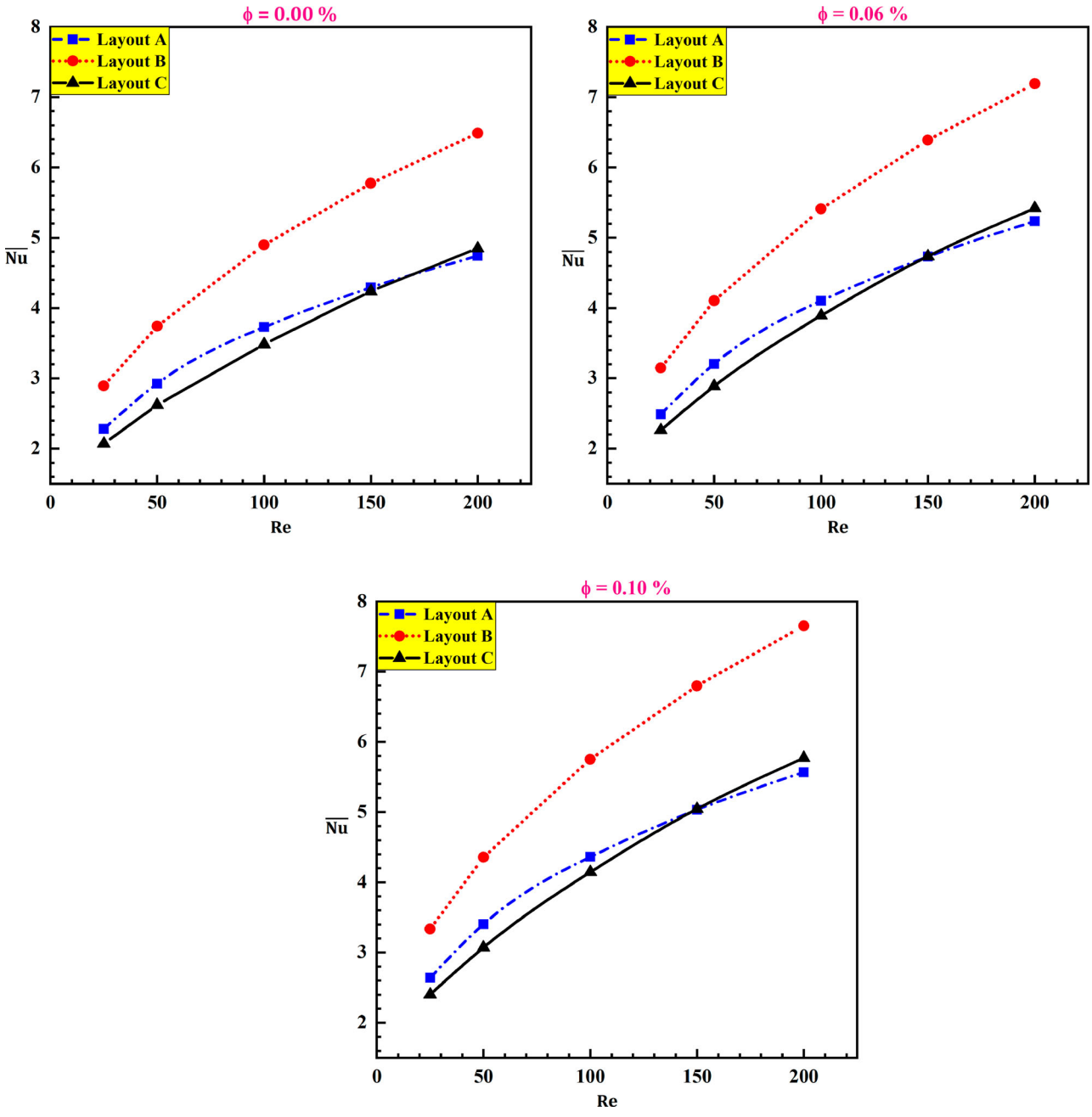

Figure 6. Variation in Nu_m at 0, 0.06 and 0.1 vol.%.

5.4. Nanoparticles volume fraction efficacy on heat exchange

In the previous section, it is observed that layout B performs better than others. In this section, the nanoparticle loading efficacy on the performance of layout B is examined. For this, $\overline{\mathrm{Nu}}$ (average Nusselt number) is computed in two scenarios. In the first scenario, the base fluid ($\varphi = 0\%$) is used and ($\overline{\mathrm{Nu}}_{\varphi=0\%}$)is computed while in the second scenario, the same computations are performed for nanofluids at 0.06 and 0.1 vol.% to obtain $\overline{\mathrm{Nu}}$. Variations in Nusselt number ratio $\frac{\overline{\mathrm{Nu}}}{\overline{\mathrm{Nu}}_{\varphi=0\%}}$ are shown in Figure 7.

The results show that in all Reynolds numbers, the presence of nanoparticles intensifies heat exchange. At 0.06 and 0.1 vol.%, heat exchanges are improved up to 10.8% and 18%, respectively.

5.5. Pumping power

Figure 7 reveals that the increases in Re and φ enhance heat exchange. ΔP is also dependent on these parameters. In Figure 8, the variation in pumping power is investigated. Increasing Re and φ exacerbate the required pumping power. Any rise in Re intensifies the shear stress

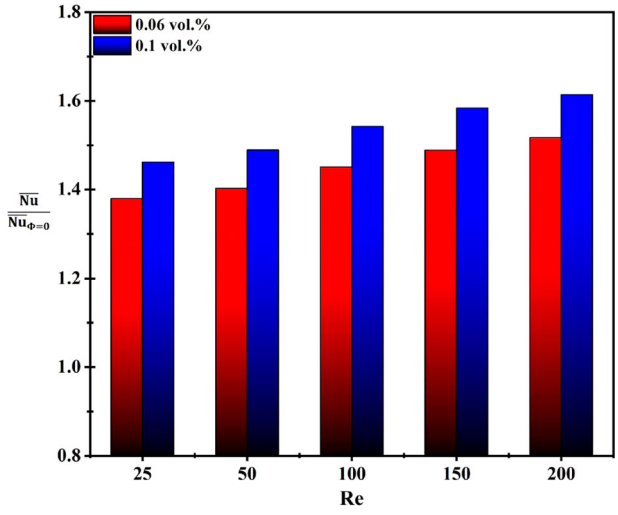

Figure 7. Effects of the presence of nanofluids in layout B.

and consequently ΔP. On the other hand, the presence of nanoparticles increases the viscosity and amplifies the shear stress and ΔP. But the presence of nanoparticles has another effect. The nanoparticle density is higher than that of the base fluid and therefore it increases the density and consequently the mass flow rate, which raises the pumping power (Equation (13)).

In Figure 8, the pumping power in layouts A, B, and C are compared. Pumping power in layout A is less than those in layouts B and C. It is because in the sinusoidal-wall layouts, the formation of vortexes intensifies ΔP and consequently increases the pumping power. Of course, another reason is the higher contact surface in the sinusoidal-wall than the smooth one.

Referring to Figure 4, it can be seen that the intensity of vortexes in layout B is higher than that in layout C, and therefore it seems logical that the pumping power of layout B should be the highest.

Figure 8 shows that sinusoidal-wall layouts (B and C) have a higher pumping power than the base one. Compared to the base one (A), the pressure drops in layouts B and C are intensified by 117% and 79%, respectively.

5.6. Figure of merit

In this section, the effects of utilizing sinusoidal-walls are examined through evaluating the figure of merit (FOM). The computations are performed in such a way that making sinusoidal wall efficacy on heat exchange and ΔP can be evaluated. Figures 6 and 8 show that layout B (sinusoidal-wall) provides more heat exchange and, at the same time, more ΔP. By evaluating FOM, we can examine the heat exchange variation relative to ΔP. As can be seen, FOM value for layout B is greater than one, while for layout C, it is less than one.

Layout C is not acceptable for two reasons. By referring to Figure 6, it can be seen that heat exchange, up to Re = 150, is less than that of layout A. ΔP is also greater, and therefore FOM parameter is always less than one (Figure 9).

5.7. Entropy generation

Entropy generation is attributed to the non-ideality of the process so that the smaller is its value, the smaller is its deviation from the ideal conditions. $\dot{s}_{gen}$ consists of thermal as well as viscous terms. The thermal term $\dot{N}_{th}$ is highly dependent on the temperature gradient and the viscous term $\dot{N}_f$ depends on the velocity gradient. In general, increasing velocity or temperature gradients lead to intensification in $\dot{N}_f$ and $\dot{N}_{th}$.

Figure 6 shows that the average Nusselt for layout B is higher than that for the other two layouts. Better heat exchange may be attributed to:

(1) Higher temperature gradient (according to Figure 4, the temperature gradient in layout B is higher than that in others)
(2) More heat transfer area.

In general, it can be claimed that the reason for the superiority of heat transfer in layout B over layout C is attributed to temperature gradient. Also, the reason for the superiority of heat exchange in layout B over layout A is attributed to temperature gradient as well as the larger heat exchange area. However, because the temperature gradient of layout B is higher than that of others, it is expected that the thermal entropy generation in layout B will be higher than that of others as shown in Figure 10.

The trend of thermal entropy changes is in accordance with Figure 6. It is seen that, up to Reynolds 150, heat exchange of layout A is better than that of layout C. As explained in the previous section, the reason for the higher heat exchange in layout A than that in layout C is attributed to the higher temperature gradient. In other words, it can be claimed that up to Re = 150, the thermal entropy generation in layout A is higher than that in layout C (owing to higher temperature gradient). However, at Re = 200, the maximum thermal entropy generation occurs. For layouts B and C, the thermal entropy generation is higher than that of the base (A) up to 35.2% and 4%, respectively.

The trend of viscous entropy generation variations is similar to Figure 8. Because the viscous entropy generation depends on the velocity gradient. In the previous section, it is mentioned (Figure 4) that the velocity gradient in layout B is higher than that of others. On the other hand, vortex formation intensifies the irreversibility of

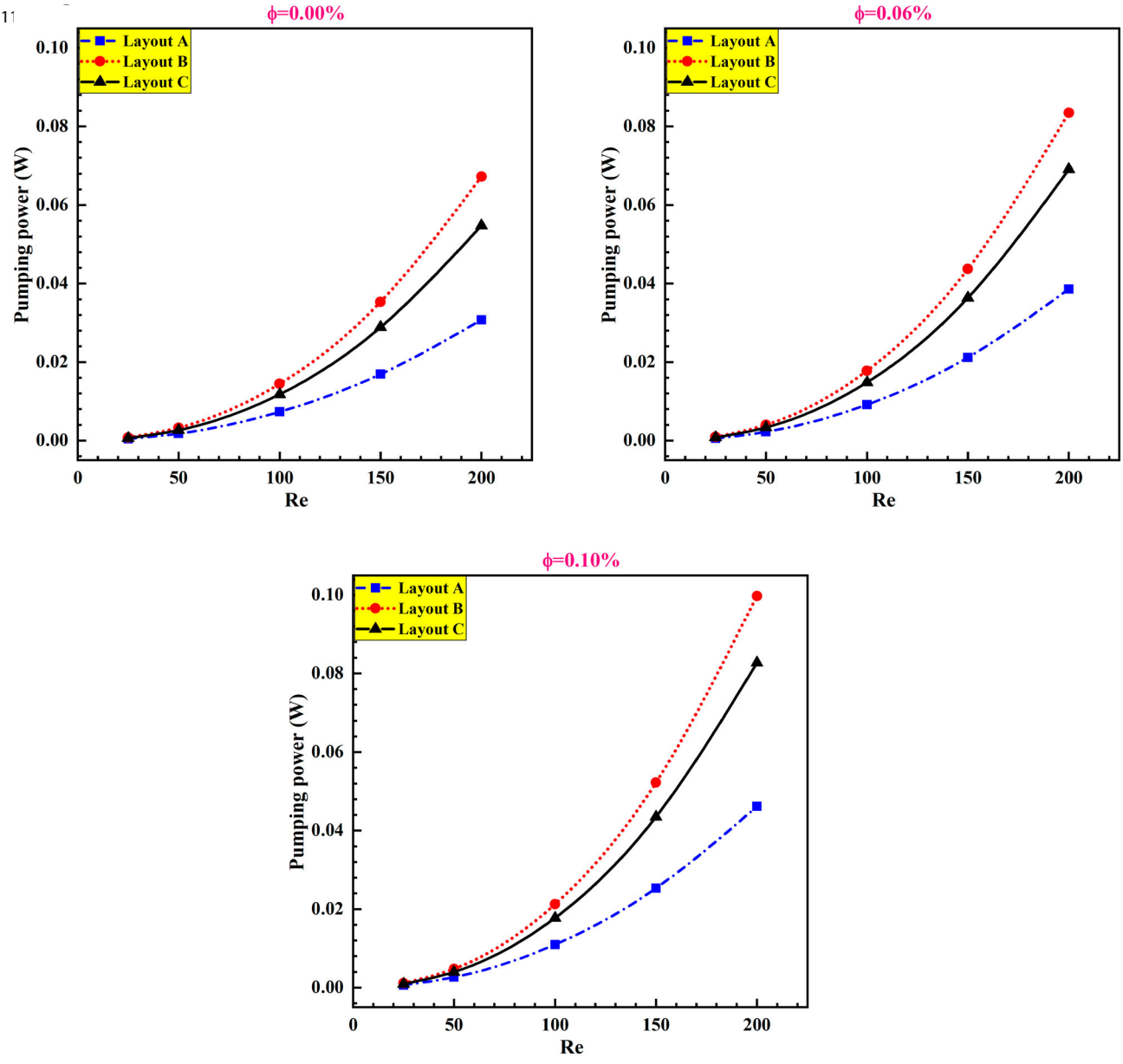

Figure 8. Pumping power sensitivity to Re and φ.

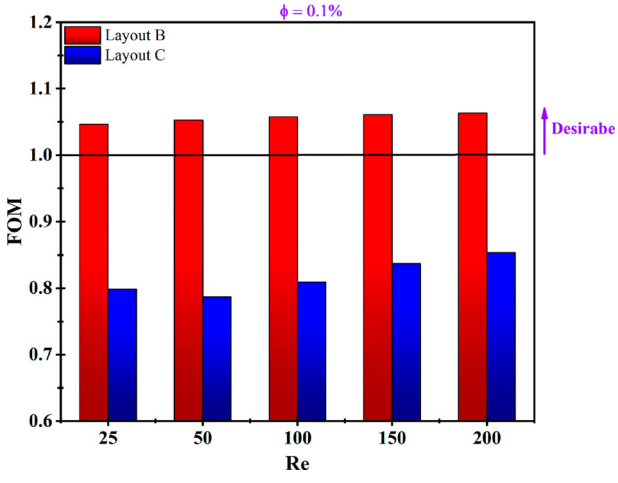

Figure 9. Evaluating FOM at 0.1 vol.%.

the system and increases the entropy generation intensity. Therefore, it is expected that layout A (due to the lower velocity gradient and lack of vortex) has the lowest viscous entropy as shown in Figure 11.

The distribution of viscous and thermal entropy generation is shown in Figure 12. It has been mentioned that layout A has a lower velocity gradient (Figure 4) and besides, no vortex is formed in this layout and therefore has the lowest viscous entropy generation. Figure 12 confirms this claim. Besides, by comparing Figures 4 and 12, it can be seen that in regions where the velocity gradient is high or the vortex is formed, there is the highest viscous entropy generation rate.

Certainly, in regions close to heating source, the temperature gradient has the highest value, and therefore the thermal entropy generation is maximum. The total

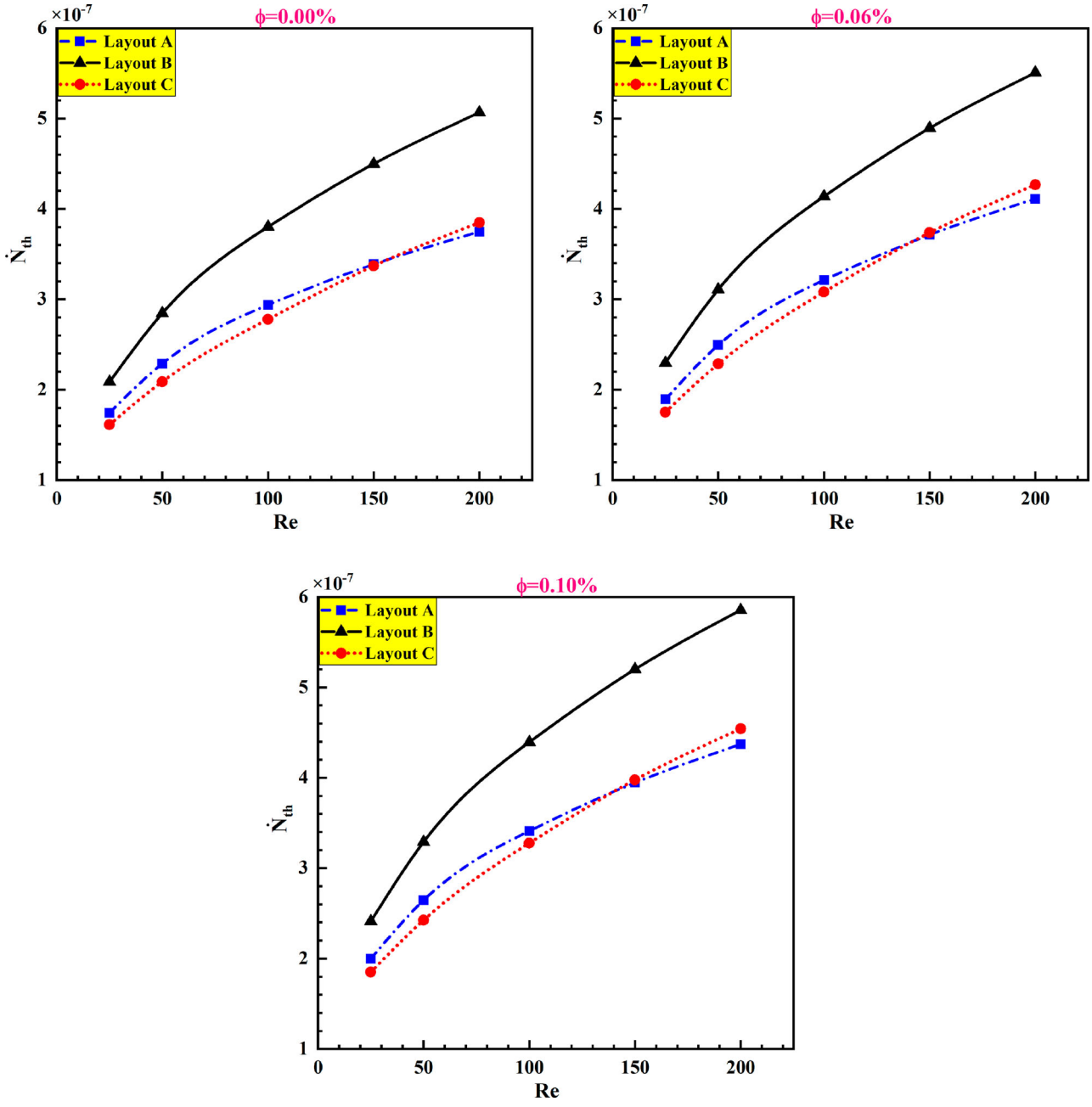

Figure 10. Thermal entropy generation comparison in three layouts.

entropy generation is obtained by summing Figures 11 and 12. On the other hand, thermal entropy generation is much higher than the viscous one (approximately 1000 times) so that the variations in total entropy generation can be considered similar to the thermal one. Therefore, it can be claimed that the total entropy generation in layouts A and B has the lowest and highest values, respectively.

6. Conclusions

Reducing the size of heat exchange units while intensifying the intensity of heat exchange is an aim that can be achieved in sinusoidal wall microchannels. In this study, the effect of heater location on the thermal and fluid performance of a microchannel with sinusoidal walls is evaluated. For this, heat exchange and ΔP of three microchannels equipped with discrete heat sources are investigated. In layout A (base), a simple microchannel with discrete heating sources is studied. In layout B, heating sources are installed in front of the converging section while in layout C, they are installed in front of the diverging section. By implementing finite volume method, heat exchange between graphene nanoplatelet /water nanofluid (0.06 and 0.1 vol.%) flow and discrete heating source is investigated at Reynolds numbers of

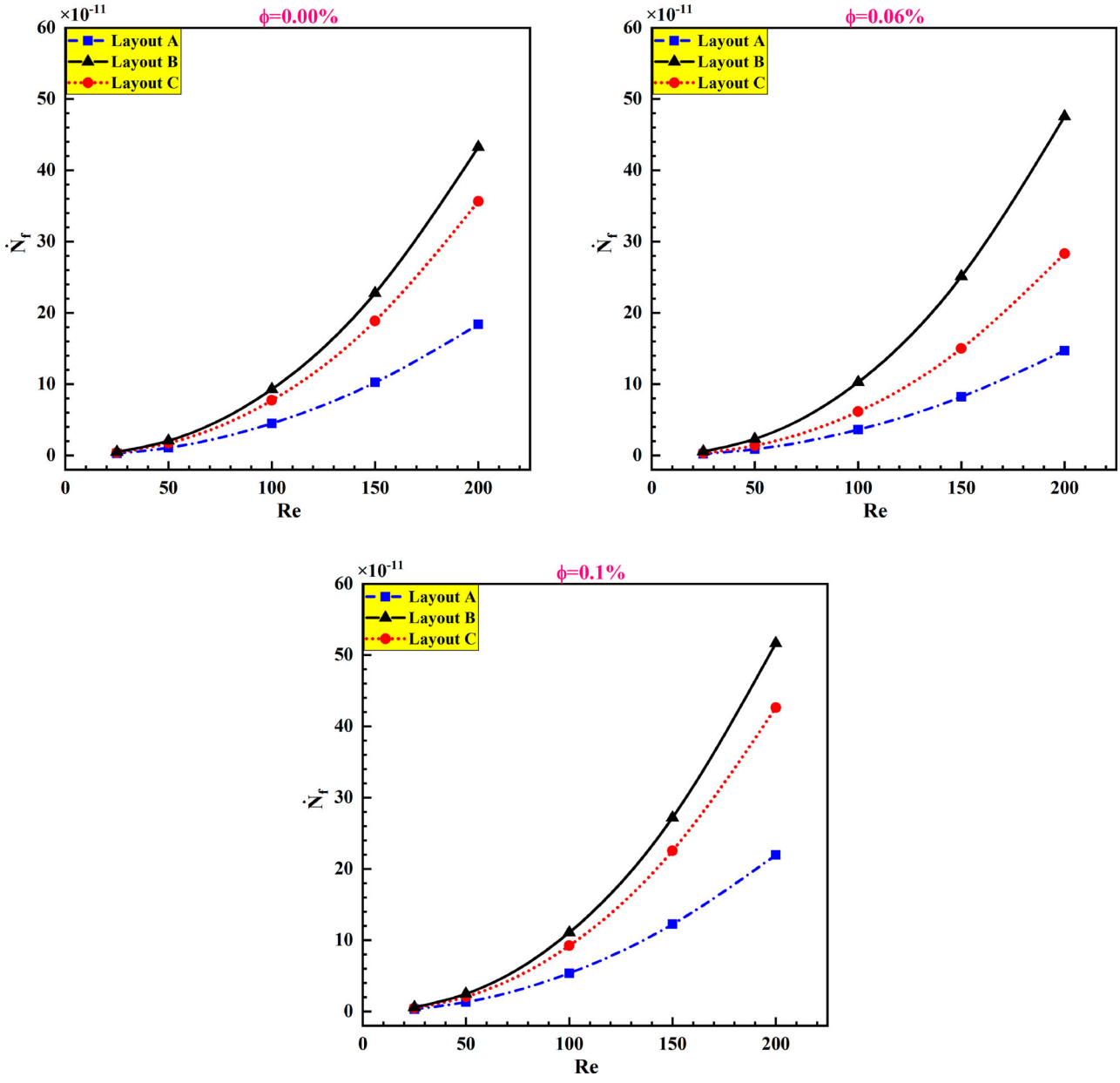

Figure 11. Viscous entropy generation comparison in three layouts

25–100. Besides, pumping power and irreversibility are compared in three layouts. The main results are:

6.1. Heat transfer

- Comparison showed that both layouts B and C are superior to layout A. The heat transfer for Layouts B and C was 1.375 and 1.037 times that of the base layout (A), respectively.
- The comparison between layout B and layout C revealed that the former layout had higher temperature gradients which consequently led to higher heat transfer potential.
- It is recommended that for sinusoidal-wall microchannel, discrete heating source should be installed in the converging section (like layout B).
- The results showed that the presence of nanoparticles intensified eat transfer. Using nanoplatelets/water nanofluid led to improvement in heat transfer by 10.8% (at 0.06 vol.%) and 18% (at 0.1 vol.%).

6.2. Pressure drop

- Although sinusoidal-wall microchannel provides more heat exchange, they also intensify pressure drop. The pressure drops in sinusoidal layouts B and C are

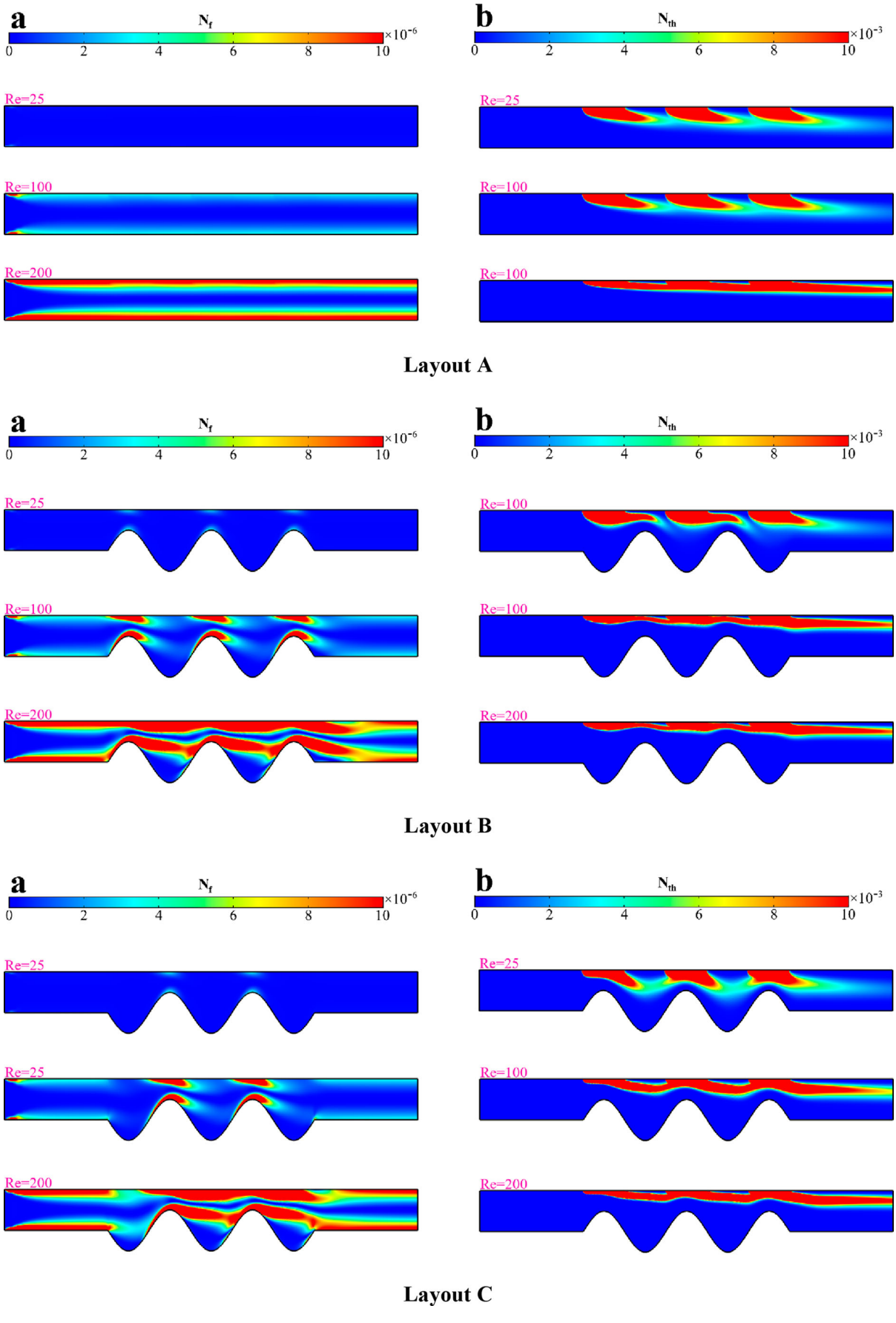

Figure 12. Viscose and thermal entropy generation in three layouts.

117% and 79% higher than that in layout A, respectively.

6.3. Entropy generation

- In all Reynolds numbers, layout B has the highest heat exchange rate as well as pumping power. Therefore, the viscous and thermal entropy generation in this layout is more than those of others. Total entropy generation in layout B is reported to be up to 35.2% higher than the base one.

Acknowledgement

This work has been financially supported by Natural Science Research Project of Guangdong University of Petrochemical Technology (519019); National Natural Science Foundation of China (21961160741); Fund of Laboratory Management Committee of Guangdong Higher Education Association (GDJ 2019054); Guangdong Science and technology projects (2021A0505060010). The open access funding is by the publication fund of the TU Dresden.

Disclosure statement

No potential conflict of interest was reported by the author(s).

Nomenclature

C_p	Specific heat $\left(\frac{\mathrm{J}}{\mathrm{kg\cdot K}}\right)$
h	Microchannel height(μm)
H	Dimensionless microchannel
l	Microchannel length(μm)
l_1, l_2, l_3, l_4	Length of insulation parts(μm)
L	Dimensionless microchannel
$\dot{N}_f$	Dimensionless frictional entropy generation
$\dot{N}_{\mathrm{th}}$	Dimensionless thermal entropy generation
Nu	Nusselt number
Pr	Prandtl number
$\bar{p}$	Pressure(Pa)
P	Dimensionless pressure
FOM	Figure of merit
$\ddot{q}$	Heat flux $\left(\frac{\mathrm{W}}{\mathrm{m}^2}\right)$
Re	Reynolds number
$\dddot{S}_f$	Frictional entropy generation $\left(\frac{\mathrm{W}}{\mathrm{m}^3\cdot\mathrm{K}}\right)$
$\dddot{S}_{\mathrm{th}}$	Thermal entropy generation $\left(\frac{\mathrm{W}}{\mathrm{m}^3\cdot\mathrm{K}}\right)$
$\dot{S}_f$	Frictional entropy generation per depth $\left(\frac{\mathrm{W}}{\mathrm{m}\cdot\mathrm{K}}\right)$
$\dot{S}_{\mathrm{th}}$	Thermal entropy generation depth $\left(\frac{\mathrm{W}}{\mathrm{m}\cdot\mathrm{K}}\right)$
T	Temperature(K)
T_c	Inlet temperature of the cold fluid stream(K)
u	Horizontal velocity $\left(\frac{\mathrm{m}}{\mathrm{s}}\right)$
u_c	Inlet nanofluid velocity $\left(\frac{\mathrm{m}}{\mathrm{s}}\right)$
U	Dimensionless horizontal velocity
v	Vertical velocity $\left(\frac{\mathrm{m}}{\mathrm{s}}\right)$
V	Dimensionless vertical velocity
x	Horizontal axis
X	Dimensionless horizontal axis
y	Vertical axis
Y	Dimensionless vertical axis

Greek symbols

φ	Volume fraction of nanoparticles(%)
μ	Dynamic viscosity(Pa · s)
θ	Dimensionless temperature
ρ	Density $\left(\frac{\mathrm{kg}}{\mathrm{m}^3}\right)$
υ	Kinematic viscosity $\left(\frac{\mathrm{m}^2}{\mathrm{s}}\right)$
α	Thermal diffusivity $\left(\frac{\mathrm{m}^2}{\mathrm{s}}\right)$

Super and subscripts

ave	Average
c	Cold
f	Fluid
h	Hot
nf	Nanofluid
s	Solid

ORCID

Dariush Bahrami http://orcid.org/0000-0001-6676-4458
Kwok-Wing Chau http://orcid.org/0000-0001-6457-161X
Amir Mosavi http://orcid.org/0000-0003-4842-0613

References

Abedi, M., Moskovskikh, D. O., Rogachev, A. S., & Mukasyan, A. S. (2016). Spark plasma sintering of titanium spherical particles. *Metallurgical and Materials Transactions B*, *47*(5), 2725–2731. https://doi.org/10.1007/s11663-016-0732-8

Akar, S., Rashidi, S., & Esfahani, J. A. (2018). Second law of thermodynamic analysis for nanofluid turbulent flow around a rotating cylinder. *Journal of Thermal Analysis and Calorimetry*, *132*(2), 1189–1200. https://doi.org/10.1007/s10973-017-6907-y

Akbari, O. A., Toghraie, D., Karimipour, A., Safaei, M. R., Goodarzi, M., Alipour, H., & Dahari, M. (2016). Investigation of rib's height effect on heat transfer and flow parameters of laminar water–Al2O3 nanofluid in a rib-microchannel. *Applied Mathematics and Computation*, *290*, 135–153. https://doi.org/10.1016/j.amc.2016.05.053

Akbarzadeh, M., Rashidi, S., Karimi, N., & Omar, N. (2019). First and second laws of thermodynamics analysis of nanofluid flow inside a heat exchanger duct with wavy walls and a porous insert. *Journal of Thermal Analysis*

and Calorimetry, *135*(1), 177–194. https://doi.org/10.1007/s10973-018-7044-y

Al Kumait, A. A., Ibrahim, T. K., & Abdullah, M. A. (2019). Experimental and numerical study of forced convection heat transfer in different internally ribbed tubes configuration using TiO2 nanofluid. *Heat Transfer—Asian Research*, *48*(5), 1778–1804. https://doi.org/10.1002/htj.21457

Babajani, M., Ghasemi, B., & Raisi, A. (2017). Numerical study on mixed convection cooling of solar cells with nanofluid. *Alexandria Engineering Journal*, *56*(1), 93–103. https://doi.org/10.1016/j.aej.2016.09.008

Bahiraei, M., Mazaheri, N., & Aliee, F. (2019). Second law analysis of a hybrid nanofluid in tubes equipped with double twisted tape inserts. *Powder Technology*, *345*, 692–703. https://doi.org/10.1016/j.powtec.2019.01.060

Bahrami, D., Nadooshan, A. A., & Bayareh, M. (2020). Numerical study on the effect of planar normal and Halbach magnet arrays on micromixing. *International Journal of Chemical Reactor Engineering*, *18*. https://doi.org/10.1515/ijcre-2020-0080

Bahrami, A., Poshtiri, A. H., & Akbarpoor, A. M. (2020). Nusselt number correlations for forced convection in a microchannel including discrete heat sources. *Journal of Thermophysics and Heat Transfer*, *34*(2), 275–286. https://doi.org/10.2514/1.T5814

Bakthavatchalam, B., Habib, K., Saidur, R., Saha, B. B., & Irshad, K. (2020). Comprehensive study on nanofluid and ionanofluid for heat transfer enhancement: A review on current and future perspective. *Journal of Molecular Liquids*, *305*, 112787. https://doi.org/10.1016/j.molliq.2020.112787

Chen, X., Zhao, T., Zhang, M.-Q., & Chen, Q. (2019). Entropy and entransy in convective heat transfer optimization: A review and perspective. *International Journal of Heat and Mass Transfer*, *137*, 1191–1220. https://doi.org/10.1016/j.ijheatmasstransfer.2019.04.017

Dinarvand, M., Abolhasani, M., Hormozi, F., & Bahrami, Z. (2021). Cooling capacity of magnetic nanofluid in presence of magnetic field based on first and second laws of thermodynamics analysis. *Energy Sources, Part A: Recovery, Utilization, and Environmental Effects*, 1–17. https://doi.org/10.1080/15567036.2021.1872746

Dormohammadi, R., Farzaneh-Gord, M., Ebrahimi-Moghadam, A., & Ahmadi, M. H. (2018). Heat transfer and entropy generation of the nanofluid flow inside sinusoidal wavy channels. *Journal of Molecular Liquids*, *269*, 229–240. https://doi.org/10.1016/j.molliq.2018.07.119

Ebrahimi, A., Roohi, E., & Kheradmand, S. (2015). Numerical study of liquid flow and heat transfer in rectangular microchannel with longitudinal vortex generators. *Applied Thermal Engineering*, *78*, 576–583. https://doi.org/10.1016/j.applthermaleng.2014.12.006

Esfahani, J., Akbarzadeh, M., Rashidi, S., Rosen, M., & Ellahi, R. (2017). Influences of wavy wall and nanoparticles on entropy generation over heat exchanger plat. *International Journal of Heat and Mass Transfer*, *109*, 1162–1171. https://doi.org/10.1016/j.ijheatmasstransfer.2017.03.006

Gravndyan, Q., Akbari, O. A., Toghraie, D., Marzban, A., Mashayekhi, R., Karimi, R., & Pourfattah, F. (2017). The effect of aspect ratios of rib on the heat transfer and laminar water/TiO2 nanofluid flow in a two-dimensional rectangular microchannel. *Journal of Molecular Liquids*, *236*, 254–265. https://doi.org/10.1016/j.molliq.2017.04.030

Heydari, M., Toghraie, D., & Akbari, O. A. (2017). The effect of semi-attached and offset mid-truncated ribs and water/TiO2 nanofluid on flow and heat transfer properties in a triangular microchannel. *Thermal Science and Engineering Progress*, *2*, 140–150. https://doi.org/10.1016/j.tsep.2017.05.010

Huminic, G., & Huminic, A. (2020). Entropy generation of nanofluid and hybrid nanofluid flow in thermal systems: A review. *Journal of Molecular Liquids*, 302, 112533. https://doi.org/10.1016/j.molliq.2020.112533

Karimipour, A., Bahrami, D., Kalbasi, R., & Marjani, A. (2020). Diminishing vortex intensity and improving heat transfer by applying magnetic field on an injectable slip microchannel containing FMWNT/water nanofluid. *Journal of Thermal Analysis and Calorimetry*, *144*, 2235–2246. https://doi.org/10.1007/s10973-020-10261-5

Kurnia, J. C., Sasmito, A. P., Shamim, T., & Mujumdar, A. S. (2016). Numerical investigation of heat transfer and entropy generation of laminar flow in helical tubes with various cross sections. *Applied Thermal Engineering*, *102*, 849–860. https://doi.org/10.1016/j.applthermaleng.2016.04.037

Kuskov, K. V., Abedi, M., Moskovskikh, D. O., Serhiienko, I., & Mukasyan, A. S. (2021). Comparison of conventional and flash spark plasma sintering of Cu–Cr pseudo-alloys: Kinetics, structure, properties. *Metals*, *11*(1), 141. https://doi.org/10.3390/met11010141

Leong, K., Saidur, R., Khairulmaini, M., Michael, Z., & Kamyar, A. (2012). Heat transfer and entropy analysis of three different types of heat exchangers operated with nanofluids. *International Communications in Heat and Mass Transfer*, *39*(6), 838–843. https://doi.org/10.1016/j.icheatmasstransfer.2012.04.003

Li, Z., Shahsavar, A., Niazi, K., Al-Rashed, A. A., & Rostami, S. (2020). Numerical assessment on the hydrothermal behavior and irreversibility of MgO-Ag/water hybrid nanofluid flow through a sinusoidal hairpin heat-exchanger. *International Communications in Heat and Mass Transfer*, *115*, 104628. https://doi.org/10.1016/j.icheatmasstransfer.2020.104628

Mazaheri, N., Bahiraei, M., Chaghakaboodi, H. A., & Moayedi, H. (2019). Analyzing performance of a ribbed triple-tube heat exchanger operated with graphene nanoplatelets nanofluid based on entropy generation and exergy destruction. *International Communications in Heat and Mass Transfer*, *107*, 55–67. https://doi.org/10.1016/j.icheatmasstransfer.2019.05.015

Min, C., Chen, J., Yang, X., Wang, K., & Xie, L. (2020). Inverse simulation to optimize the rib-profile in a rectangular flow-channel. *International Communications in Heat and Mass Transfer*, *114*, 104567. https://doi.org/10.1016/j.icheatmasstransfer.2020.104567

Nguyen, Q., Bahrami, D., Kalbasi, R., & Karimipour, A. (2020). Functionalized multi-walled carbon nano tubes nanoparticles dispersed in water through an magneto hydro dynamic nonsmooth duct equipped with sinusoidal-wavy wall: Diminishing vortex intensity via nonlinear Navier–Stokes equations. *Mathematical Methods in the Applied Sciences*, 7(11). https://doi.org/10.1002/mma.6528

Rashidi, S., Zade, N. M., & Esfahani, J. A. (2017). Thermo-fluid performance and entropy generation analysis for a new eccentric helical screw tape insert in a 3D tube. *Chemical Engineering and Processing: Process Intensification*, *117*, 27–37. https://doi.org/10.1016/j.cep.2017.03.013

Ravi, B. V., Singh, P., & Ekkad, S. V. (2017). Numerical investigation of turbulent flow and heat transfer in two-pass ribbed channels. *International Journal of Thermal Sciences*, *112*, 31–43. https://doi.org/10.1016/j.ijthermalsci.2016.09.034

Ren, X.-H., Liu, R.-Z., Wang, Y.-H., Wang, L., & Zhao, F.-Y. (2019). Thermal driven natural convective flows inside the solar chimney flush-mounted with discrete heating sources: Reversal and cooperative flow dynamics. *Renewable Energy*, *138*, 354–367. https://doi.org/10.1016/j.renene.2019.01.090

Sankar, M., & Do, Y. (2010). Numerical simulation of free convection heat transfer in a vertical annular cavity with discrete heating. *International Communications in Heat and Mass Transfer*, *37*(6), 600–606. https://doi.org/10.1016/j.icheatmass-transfer.2010.02.009

Shamsi, M. R., Akbari, O. A., Marzban, A., Toghraie, D., & Mashayekhi, R. (2017). Increasing heat transfer of non-Newtonian nanofluid in rectangular microchannel with triangular ribs. *Physica E: Low-Dimensional Systems and Nanostructures*, *93*, 167–178. https://doi.org/10.1016/j.physe.2017.06.015

Shen, B., Yan, H., Sunden, B., Xue, H., & Xie, G. (2017). Forced convection and heat transfer of water-cooled microchannel heat sinks with various structured metal foams. *International Journal of Heat and Mass Transfer*, *113*, 1043–1053. https://doi.org/10.1016/j.ijheatmasstransfer.2017.06.004

Shiriny, A., Bayareh, M., Nadooshan, A. A., & Bahrami, D. (2019). Forced convection heat transfer of water/FMWCNT nanofluid in a microchannel with triangular ribs. *SN Applied Sciences*, *1*(12), 1631. https://doi.org/10.1007/s42452-019-1678-7

Toghraie, D., Mashayekhi, R., Arasteh, H., Sheykhi, S., Niknejadi, M., & Chamkha, A. J. (2019). Two-phase investigation of water-Al2O3 nanofluid in a micro concentric annulus under non-uniform heat flux boundary conditions. *International Journal of Numerical Methods for Heat & Fluid Flow*, *30*(4), 1795–1814. https://doi.org/10.1108/HFF-11-2018-0628

Vatanparast, M. A., Hossainpour, S., Keyhani-Asl, A., & Forouzi, S. (2020). Numerical investigation of total entropy generation in a rectangular channel with staggered semi-porous fins. *International Communications in Heat and Mass Transfer*, *111*, 104446. https://doi.org/10.1016/j.icheatmass-transfer.2019.104446

Wang, C.-C., & Chen, C.-K. (2002). Forced convection in a wavy-wall channel. *International Journal of Heat and Mass Transfer*, *45*(12), 2587–2595. https://doi.org/10.1016/S0017-9310(01)00335-0

Xu, H. J., Xing, Z. B., Wang, F., & Cheng, Z. (2019). Review on heat conduction, heat convection, thermal radiation and phase change heat transfer of nanofluids in porous media: Fundamentals and applications. *Chemical Engineering Science*, *195*, 462–483. https://doi.org/10.1016/j.ces.2018.09.045

Yang, L., Huang, J.-N., Mao, M., & Ji, W. (2020). Numerical assessment of Ag-water nano-fluid flow in two new microchannel heatsinks: Thermal performance and thermodynamic considerations. *International Communications in Heat and Mass Transfer*, *110*, 104415. https://doi.org/10.1016/j.icheatmasstransfer.2019.104415